Evaluation of Modified Median Root Prior on a myocardium study, using realistic PET/MR data

Konstantinos Karaoglanis, Anastasios Gaitanis, Charalampos Tsoumpas

Abstract— **One way of treating the partial volume effect in PET image reconstruction is by using anatomical information from other imaging modalities (MRI or CT). The *a priori* information of a maximum a posteriori reconstruction algorithm is defined from the anatomical images. In this paper the ordered subsets modified median root prior one step late (OS-MMRP-OSL) algorithm [1], which uses information derived from MR images, is evaluated in a computationally simulated PET FDG myocardium study. The algorithm was implemented in STIR (Software for Tomographic Image Reconstruction) [2], (http://stir.sourceforge.net). Realistic PET data have been used, to compare the standard ordered subsets median root prior one step late (OS-MRP-OSL) algorithm with the OS-MMRP-OSL algorithm using well-aligned segmented and non-segmented MR images. In some cases the quantitative results indicate lower bias (by 6.5%) for OS-MMRP-OSL using segmented MR images and decreased root mean square error (RMSE) by 3%. Moreover, we have improvement in edge preservation.**

I. Introduction

Statistical iterative reconstruction algorithms (MLEM and OSEM) are used mainly in emission tomography (PET & SPECT) and they allow better physics modeling but noise propagation over iterations still remains an issue. Widely used noise reduction techniques like post-filtering and early stopping of iterative algorithms are palliatives as they result in various problems like higher bias or low resolution due to over smoothing. Maximum a Posteriori (MAP) methods introduce prior probability density functions which improve the convergence speed and reduce noise [3]. MAP methods can be space invariant or they can use anatomical information from other modalities.

Bettinardi et al [4] evaluated the space invariant ordered subsets maximum a posterior one step late algorithm (OSMAPOSL) with median root prior (OS-MRP-OSL) showing that the algorithm can reach a stable solution with good spatial resolution and noise reduction.

Manuscript received July 9, 2013. This work was supported by the European Union COST Action TD1007 (http://www.pet-mri.eu/).

K Karaoglanis was in Department of Biomedical Technology, Biomedical Research Foundation of the Academy of Athens (BRFAA), Soranou Efessiou 4, Athens and Division of Imaging Sciences and Biomedical Engineering, Department of Biomedical Engineering, King's College London, King's Health Partners, St. Thomas' Hospital, London SE1 7EH, UK (email: karaoglankwnst@windowslive.com)

A Gaitanis is with the Department of Biomedical Technology, Biomedical Research Foundation of the Academy of Athens (BRFAA), Soranou Efessiou 4, Athens. (corresponding author to provide phone: +30-210-6597318; fax: +30-210-6597629; e-mail: agaitanis@bioacademy.gr).

C Tsoumpas is with the Division of Imaging Sciences and Biomedical Engineering, Department of Biomedical Engineering, King's College London, King's Health Partners, St. Thomas' Hospital, London SE1 7EH, UK (email: charalampos.tsoumpas@kcl.ac.uk)

The correlation between tracer concentration and the underlying anatomy is considered to form priors guided by anatomical information in both PET and Single Photon Emission Computed Tomography (SPECT) [5]. Anatomical priors can be derived from Magnetic Resonance Imaging (MRI) or Computed Tomography (CT) images. Cheng-Liao et al [6] used anatomical information from CT images using Level Set Functions guided by an automated edge detector, showing promising results.

Vunckx et al [7] evaluated a modified Bowsher algorithm [8] using non-segmented MRI images for PET brain images. This study showed better bias and noise reduction compared to post-smoothed MLEM and the standard version of the prior. Caldeira et al [1] developed a modified version of the OS-MRP-OSL using anatomical information from MRI images (OS-MMRP-OSL). This brain study showed lower values of RMSE and noise reduction compared to OSEM and the space invariant version of the algorithm. Moreover, OS-MRP-OSL produced images with contrast values similar to OSEM. In another study, Caldeira et [9] al compared the OS-MMRP-OSL with the Bowsher prior. The comparison showed that the bowsher prior achieves better mean square error and coefficient of variation.

The most demanding aspect when using prior information from MR images is the segmentation and the accurate alignment. In this work, we evaluate the OS-MMRP-OSL algorithm in a simulated FDG PET myocardium study. We compare the standard and modified version of algorithms in a quantitative way. In myocardium studies, edge preservation is crucial as it is surrounded by various other structures. Moreover techniques like post-filtering cause smoothing at the edges that affect the shape of the myocardium. We also examine the effect of misalignment and the use of un-segmented MR images.

II. Materials and Methods

A. Algorithm

The ordered subsets maximum a posterior one step late (OSMAPOSL) algorithm using Median Root Prior (MRP) has been described by Alenius et al [10]. The original OSL algorithm was developed by Green [11, 12] and was implemented in STIR [2]. The MAP method can be described as a filter applied to the update image. The OS-MRP-OSL algorithm is given by the following formula:

$$\lambda_{OSL}^{new} = \frac{1}{1+\beta\frac{\lambda(i)-Med(\lambda,i)}{Med(\lambda,i)}\,|\,\lambda=\lambda_{OSL}^{old}}\lambda_{OSEM}^{new} \quad (1)$$

Where, i is the pixel, β is the weight of the MRP (penalization factor), $Med(\lambda,i)$ is the median of a block of neighbor pixels (e.g. 3×3×3, 5×5×5, etc) and λ is the image.

978-1-4799-3163-7/13/$31.00 ©2013 IEEE

The modified version of the algorithm using information from MR is described by the following formula [1]:

$$\lambda^{(n+1)} = \frac{\lambda_i^n}{\sum_i p_{ij} + \beta \frac{\lambda_i^n - M_i}{M_i}} \sum_j \frac{y_j p_{ij}}{\sum_k p_{kj} \lambda_k^{(n)}} \quad (2)$$

Where, p_{ij} is the system matrix, y_j is the number of coincidences in detector pair j, λ_i indicates the activity of voxel i, M_i is the median of the neighbor voxels of voxel i (defined as a kernel with a certain size e.g. 3×3×3 or 5×5×5) and β is the weight of the prior.

The main difference of the two aforementioned algorithms is the way kernels are formed around voxel i, in order to calculate the median. In the case of standard MRP (OS-MRP-OSL) all pixels around voxel i are used to calculate the median without taking into account their value or any other information. On the other hand, in the modified version (OS-MMRP-OSL) the MR image is taken into account in order to define which of the pixels around voxel i belong to the same tissue and thus is taken into consideration for the calculation of median. Therefore, it is expected the two versions will work in the same manner in uniform areas. Conversely, OS-MMRP-OSL is expected to create PET images with sharper edges at the boundaries of MR-defined anatomical regions. Caldeira et al [1] unveiled the fact that the algorithm achieves lower bias and RMSE especially for large kernels. Moreover, better contrast and preserving details at the edges of the anatomical regions have been observed.

In this investigation, we evaluate the algorithm in a simulated FDG PET myocardium study and compare the modified version with the standard one.

B. Simulated PET data and real MR images

Tsoumpas et al [13] described a technique to produce realistic PET data from MR images. Through a fast analytic simulation, a PET acquisition was simulated including scatter, attenuation and resolution effects [13, 14]. The simulated scanner was the Philips Gemini. During this project, we used a data set corresponding to 42.2 million counts including scattered events.

The dynamic MR image, which was acquired through a T1-weighted TFE sequence, was modified in order to have the same matrix and voxel size with the PET data. The image was segmented as described elsewhere [13]. The segmented MR images indicate six different anatomic areas (air, liver, lung, soft tissue, bone and myocardium).

C. Reconstruction Setup

For both OS-MRP-OSL and OS-MMRP-OSL algorithms, reconstructions were performed for 50 iterations with 2 subsets. The size of images was 250×250×87 with 2mm voxel size. As initial estimate, a uniform image was used. The voxel values of this image were defined by dividing the total counts with the number of voxels. The kernel size was 3×3×3 voxels in all cases. The segmented MR image has been used twice, one perfectly aligned and one with a minor misalignment. Finally, various penalization factors were used (β=0.5, 1, 5, 10, 40, 50, 60, 75, 100).

III. RESULTS

Firstly, the behavior of the algorithms in terms of RMSE was analyzed. The top row of Figure 1 shows that for all penalization factors RMSE is decreased until a certain iteration that is between 15th and 20th. After this, RMSE is gradually increasing. When OS-MRP-OSL with large penalization factor (>10) is used, RMSE continues to decrease even after 20 iterations. In early iterations (<10) the RMSE values for both algorithms and the anatomical images deployed are the same.

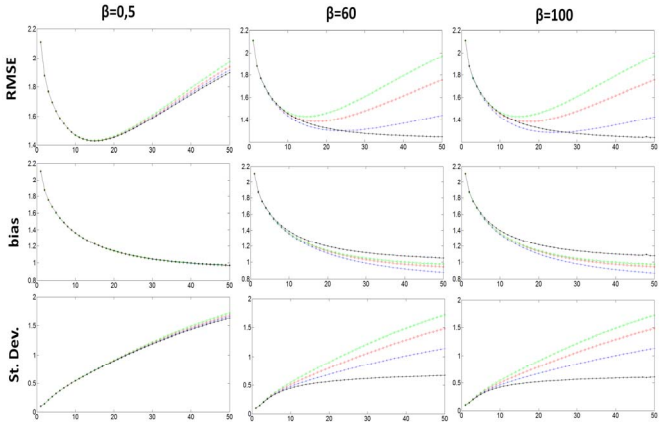

Fig.1 RMSE (First row), bias (Second row), Standard Deviation (Third row) vs. iterations for the myocardium. Results for different penalization factors β=0.5 (First column), β=60 (Second column) and β=100 (Third column). Blue line: OS-MMRP-OSL using the segmented MR image which is aligned. Red line: OS-MMRP-OSL using the segmented MR image which is slightly misaligned. Green line: OS-MMRP-OSL using the un-segmented MR image. Black line: standard version of the algorithm (OS-MRP-OSL).

This can be verified from figure 2 where we can observe that for early iterations the images are very similar. After 20th iteration, the differentiation between the methods is observed. For low penalization values, the differentiation is minor as the effect of the prior is small. As the value of the penalization factor increases, the differentiation between the methods is more intense. OS-MRP-OSL achieves overall the lowest RMSE but for late iterations. OS-MMRP-OSL using the perfectly aligned segmented MR image achieves lower RMSE between 10th and 20th iterations. The OS-MMRP-OSL using misaligned-segmented MR image achieves considerably higher RMSE. This fact becomes more pronounced, as the effect of the prior is more intense.

In the second row of figure 1**,** the bias over the iterations is shown. Bias decreases steadily for all β over iterations. The differentiation between the studied methods is observed after a certain number of iterations and it is more noticeable as higher penalization factors are deployed. Similar results for accuracy can be visually observed in figure 3. OS-MMRP-OSL using the perfectly aligned segmented image steadily achieves the lowest bias. The modified algorithm achieves lower bias regardless of which MR image is used. In the results of the modified algorithm using the un-segmented MR image, it is observed that, the bias was higher, which becomes more than 10% higher than the optimum for late iterations and high penalization factors.

When examining the effect of misalignment, we notice that the results deteriorate due to the disposition.

In the third row of figure 1 the behavior of standard deviation over iterations is shown. Standard deviation steadily increases when an anatomical prior is deployed. The standard deviation of OS-MRP-OSL images steadily increases, for all β. OS-MRP-OSL achieves the lowest standard deviation.

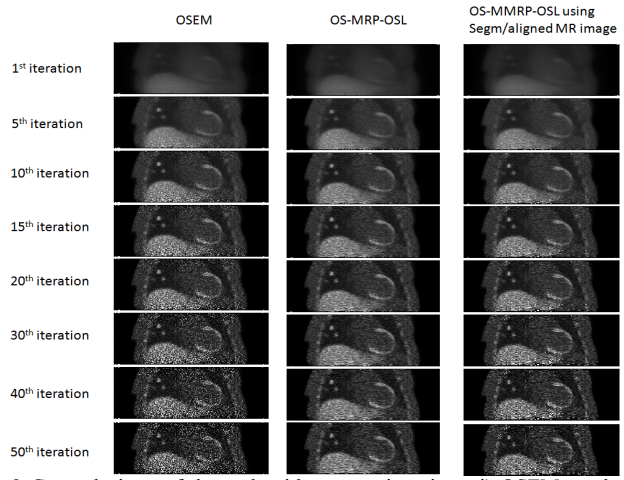

Fig. 2 Coronal views of three algorithms over iterations: i) OSEM results (left column), ii) OS-MRP-OSL with β=60 (middle column), iii) OS-MMRP-OSL with β=60 using the perfectly aligned and segmented MR image (right column). Min=0 and max=5

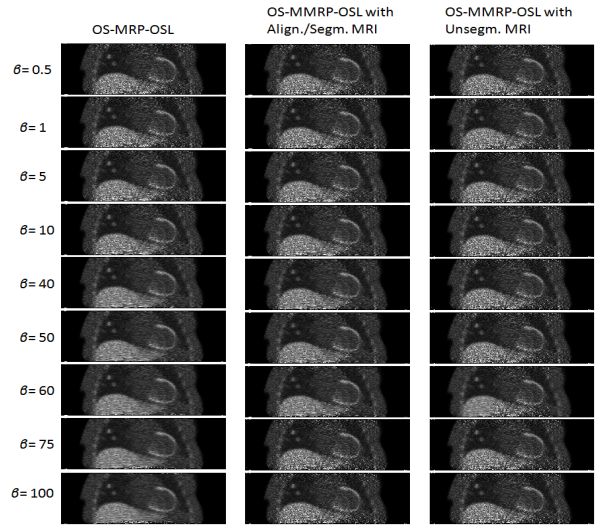

Fig. 3 Coronal views of three algorithms after 15 iterations; OS-MRP-OSL (Left column). OS-MMRP-OSL using the perfectly aligned and segmented MR image (Middle column) . OS-MMRP-OSL using the un-segmented MR image (Right column). Min=0, max=5.

Once again, one can observe that the use of a misaligned-segmented MR image gives higher standard deviation than the aligned one and that the un-segmented gives the worst results. When a low penalization factor is used (β=0.5 and 1) the results are similar. Another interesting observation is that for high β (>10) the difference between the two methods is not affected by the increasing penalization factor.

Taking into account the results, we decided to investigate further the reconstructed images at the 15th iteration. At this iteration the lowest RMSE is achieved for most β, the standard deviation has not increased so much and bias is at an acceptable level. In figure 4, the bias over standard deviation can be observed. Each point corresponds to a different penalization factor. For the OS-MRP-OSL the increased penalization factor results in lower standard deviation but at the same time bias increases. When the algorithm incorporates anatomical information the bias decreases along with standard deviation as the effect of the increased prior (higher β). When a misaligned and segmented MR image is used, the decrease of the aforementioned factors is not as intense as when the aligned and segmented image is used. When the modified version of the algorithm uses the un-segmented MR image there seems to be no variations using different penalization factors.

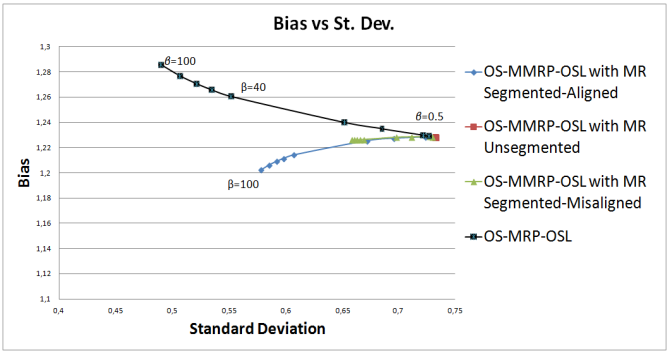

Fig. 4 Bias versus standard deviation for the myocardium image after 15 iterations. Each spot corresponds to different penalization factor. Red line: OS-MMRP-OSL using the un-segmented MR image. Green line: OS-MMRP-OSL using the segmented MR image, which is slightly misaligned. Blue line: OS-MMRP-OSL using the perfectly aligned, segmented MR image. Black line: standard version of the algorithm OS-MRP-OSL.

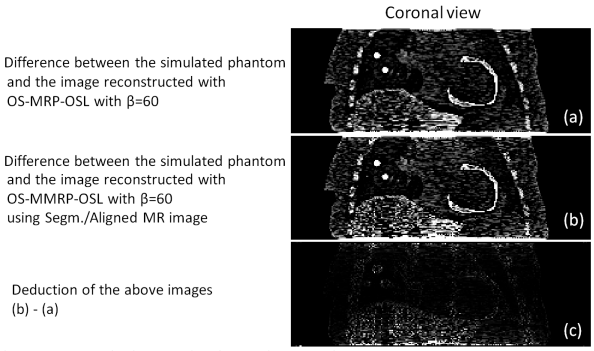

Fig. 5 Coronal views of subtractions. Min=0, Max=1

In the case of OS-MRP-OSL, RMSE deteriorates for all β between 0 and 60 while it increases for higher β. When the modified version is used with segmented MR images, the RMSE steadily decreases for all penalization factors. The misalignment causes worst results; in the case of β=60, the RMSE is increased by 3.7%, due to the misalignment. OS-MMRP-OSL with the segmented and aligned MR image achieves lower RMSE values than the OS-MRP-OSL, but the use of a misaligned image provides deteriorated results than the OS-MRP-OSL.

The ability of the modified version of the algorithm to preserve myocardium edges is shown in figure 5. In this

figure, images illustrate the difference between the simulated PET phantom and their reconstructed images with OS-MRP-OSL and OS-MMRP-OSL after 15 iterations. Through a visual inspection, it is noticed that (b) is less noisy with more details shown. To further investigate this fact we use image (c) which is the result of subtracting image (a) from (b). In image (c), it is seen that the difference between the two images is at the borders of the anatomical regions (myocardium), showing the algorithm's ability to preserve the boundaries.

IV. Discussion

The results indicate that the reconstructed images of the two algorithms differ for large penalization factors (>10) and after a certain number of iterations (>6). Firstly, the two algorithms were compared. For the modified version, the well aligned-segmented MR image used as anatomical map. For both algorithms the behavior of the RMSE is similar. For early iterations (9^{th}-18^{th}), OS-MMRP-OSL achieves lower RMSE values than OS-MRP-OSL (Figure 1: first row). At later iterations the noise increases for the modified algorithm, while OS-MRP-OSL produces images with lower noise (Figure 1: third row). Moreover, the images reconstructed with the OS-MMRP-OSL seem to be more noisy but with more details shown (Figure 3). When an anatomical map is used, lower bias is observed even if un-segmented or misaligned MR images are employed (Figure 1: second row). This difference in the accuracy can be justified by the improved results obtained in the anatomical boundaries. The fact that OS-MMRP-OSL works in the boundaries, as expected, is illustrated in figure 5(c). In this figure we can see that positive values derived from OS-MRP-OSL are obtained around the edges, due to the diffusion of activity caused by the median calculation. The images from the two algorithms have different values at the edges of anatomical regions, while no variations are observed at uniform areas.

Moreover, we compare the use of different anatomical maps for the OS-MMRP-OSL. It is obvious that the results deteriorate with the un-segmented MR image. Figure 4 shows, that no variations are observed as the penalization factor increases. This can be justified because the algorithm takes into consideration the values of the anatomical map as absolute values. Due to the fact that the values in the un-segmented MR images are diversified even in the same anatomical regions, few voxel values are taken into account to compute the mean. Misalignment deteriorates the results for all examined β. As aforementioned, the diversification on the way the two algorithms work is focused at the edges and misalignment removes any advantage of the modified version.

V. Conclusion

The modified version of the iterative reconstruction algorithm using the well aligned/segmented MR image produces lower RMSE values at early iterations. Moreover, OS-MMRP-OSL is more accurate showing more detailed and sharper edges. In the images acquired from the standard version of the algorithm, lower standard deviation and less noisy images have been observed. OS-MMRP-OSL does not perform very well with the un-segmented images and a modification of the algorithm is needed. We have also observed the results of misalignment, which deteriorates the performance of the OS-MRP-OSL.

Acknowledgment

The simulated PET-MR data have been obtained from the website: http://www.isd.kcl.ac.uk/pet-mri/simulated-data/.
The authors would like to thank Drs. G. Spyrou, C. Anagnostopoulos and G. Kastis for the useful suggestions and fruitful discussions.

References

[1] L. Caldeira, J. J. Scheins, P. Almeida, J. Seabra, and H. Herzog, "Modified Median Root Prior reconstruction of PET/MR data acquired simultaneously with the 3TMR-BrainPET," in Nuclear Science Symposium and Medical Imaging Conference (NSS/MIC), 2011 IEEE, pp. 4039-4043, 2011.

[2] K. Thielemans, C. Tsoumpas, S. Mustafovic, T. Beisel, P. Aguiar, N. Dikaios, et al., "STIR: software for tomographic image reconstruction release 2," Phys Med Biol, vol. 57, pp. 867-83, 2012.

[3] J. Qi and R. M. Leahy, "Iterative reconstruction techniques in emission computed tomography," Phys Med Biol vol. 51, p. R541, 2006.

[4] V. Bettinardi, E. Pagani, M. C. Gilardi, S. Alenius, K. Thielemans, M. Teras, et al., "Implementation and evaluation of a 3D one-step late reconstruction algorithm for 3D positron emission tomography brain studies using median root prior," Eur J Nucl Med Mol Imaging, vol. 29, pp. 7-18, 2002.

[5] S. Kulkarni, P. Khurd, I. Hsiao, L. Zhou, and G. Gindi, "A channelized Hotelling observer study of lesion detection in SPECT MAP reconstruction using anatomical priors," Phys Med Biol, vol. 52, p. 3601, 2007.

[6] J. Cheng-Liao and J. Qi, "PET image reconstruction with anatomical edge guided level set prior," Phys Med Biol, vol. 56, p. 6899, 2011.

[7] K. Vunckx and J. Nuyts, "Heuristic modification of an anatomical Markov prior improves its performance," in Nuclear Science Symposium Conference Record (NSS/MIC), 2010 IEEE, 2010, pp. 3262-3266.

[8] J. E. Bowsher, Y. Hong, L. W. Hedlund, T. G. Turkington, G. Akabani, A. Badea, et al., "Utilizing MRI information to estimate F18-FDG distributions in rat flank tumors," in Nuclear Science Symposium Conference Record, 2004 IEEE, 2004, pp. 2488-2492 Vol. 4.

[9] L. Caldeira, J. Scheins, P. Almeida, and H. Herzog, "Evaluation of two methods for using MR information in PET reconstruction," Nuclear Instruments and Methods in Physics Research Section A: Accelerators, Spectrometers, Detectors and Associated Equipment, vol. 702, pp. 141-143, 2013.

[10] S. Alenius, U. Ruotsalainen, and J. Astola, "Using local median as the location of the prior distribution in iterative emission tomography image reconstruction," IEEE Trans Nucl Sci on, vol. 45, pp. 3097-3104, 1998.

[11] P. J. Green, "Bayesian reconstructions from emission tomography data using a modified EM algorithm," IEEE Trans Med Imaging, vol. 9, pp. 84-93, 1990.

[12] P.J. Green, "On Use of the EM Algorithm for Penalized Likelihood Estimation", Journal of the Royal Statistical Society. vol. 52, 3p. 443-452, 1990.

[13] C. Tsoumpas, C. Buerger, A. P. King, P. Mollet, V. Keereman, S. Vandenberghe, et al., "Fast generation of 4D PET-MR data from real dynamic MR acquisitions," Phys Med Biol, vol. 56, pp. 6597-613, 2011.

[14] C. Tsoumpas, I. Polycarpou, K. Thielemans, C. Buerger, A. P. King, T. Shaeffter, et al., "The effect of regularization in motion compensated PET image reconstruction: a realistic numerical 4D simulation study," Phys Med Biol, vol. 58, pp. 1759-73, 2011